



# Pumping with electroosmosis of the second kind in mesoporous skeletons

Fevzi C. Kivanc, Shawn Litster\*

Dept. of Mechanical Engineering, Carnegie Mellon University Pittsburgh, Scaife Hall 323, 5000 Forbes Ave, Pittsburgh, PA, 15213, United States

## ARTICLE INFO

### Article history:

Received 7 June 2010

Received in revised form 9 August 2010

Accepted 14 September 2010

Available online 7 October 2010

### Keywords:

Electroosmotic pump

Electroosmosis of the second kind

Nonlinear electrokinetics

Micropump

Mesoporous silica

Mesoporous skeleton

## ABSTRACT

This paper presents the use of mesoporous silica skeletons as substrates for electroosmotic (EO) micropumps. Mesoporous silica skeletons have bimodal pore size distributions consisting of macropores and cation-permselective mesopores. These materials have the potential for high flow rate per power because the cation-permselective mesopores can generate an induced charge layer (ICL) and electroosmosis of the second kind (EO-2) under high applied electric fields. The diffuse charge layers induced by the electric field result in an EO-2 flow rate that increases quadratically with increasing electric field. In contrast, the flow rate of the more common electroosmosis of the first kind (EO-1) is linearly proportional to electric field. Here, we investigate the impact of finite pressure loads on the EO-2 flow rate with experiments and an engineering model to evaluate the potential of mesoporous skeletons for micropumping applications. Our results include analyses of maximum flow rate, maximum pressure, and flow rate with intermediate pressure loads. The results indicate the existence of a critical pressure load at which reverse pressure-driven flow significantly diminishes the EO-2 flow. We also investigate the scaling of flow rate per power with respect to substrate thickness and area, demonstrating significant increases in flow rate per power with thinner substrates and favorable scaling for miniaturization of EO-2 pumps.

© 2010 Elsevier B.V. All rights reserved.

## 1. Introduction

EO pumps are well-suited to micropumping applications because they feature no moving parts, low power requirements, and high self-pumping frequencies [1]. EO pumps are receiving increasing interest for several applications, including micro-processor cooling, drug delivery, and fuel cells [2–4]. EO pumps are commonly based on porous substrates because of the high density of small pores that generate significant flow under a wide range of pressure loads. Most EO pumps based on porous substrates rely on EO-1. EO-1 arises because of the native surface charge and electric double layers (EDLs) that develop at solid/liquid interfaces. When an external electric field is applied, it imposes a Lorentz force on the EDL's diffuse layer of charge in the liquid, driving bulk flow through viscous interaction. For EO-1, the flow rate is proportional to the substrate area and varies linearly with the electric field.

Nischang and Tallarek [5] demonstrated that the EO flow rate with mesoporous silica skeletons varies quadratically with electric field (under zero pressure load) due to non-linear electrokinetic phenomena. They attributed this behavior to the ICL generated by the mesopores and the resulting EO-2 flow. In contrast to EO-1, the EO-2 flow rate varies nonlinearly with electric field

because additional diffuse charge is induced by concentration polarization (CP) [6]. CP is the formation of ion concentration gradients in the working fluid at the boundary of ion-permselective media under an applied electric field. Ion-permselectivity arises due to the significant excess of mobile counter-ions shielding immobile surface charges when electric double layer thicknesses approach the pore diameter. Thus, the current in ion-permselective pores is primarily carried by the counter-ion, resulting in species electromigration flux imbalances that induce CP at the interfaces between ion-permselective media and bulk solutions. For the cation-permselective mesoporous silica skeleton illustrated in Fig. 1, the anions are driven by the electric field to the cathode side of the skeleton, but cannot enter it because of significant overlap of the mesopore EDLs. On the anode side, the electric field pulls anions away from the surface of the skeleton. Thus, the electric field produces an enrichment zone at the cathodic interface as anions and cations accumulate (cations for electroneutrality). At the anodic interface, a depletion region forms. At high electric fields, a layer of induced charge (the ICL) develops on the anodic interface because anions are removed from the depletion region while cations enter the depletion zone from the mesopores. The applied electric field imposes a Lorentz force on the ICL and generates EO-2 flow. For additional background information, the interested reader is referred to the article by Nischang et al. [7].

Recently, Mishchuk et al. [8] presented a micropump that used EO-2 around 50  $\mu\text{m}$  diameter ion exchange beads placed in a micro-channel. In agreement with their model, this micropump exhibited

\* Corresponding author. Tel.: +1 412 268 3050; fax: +1 412 268 3348.  
E-mail address: [litster@andrew.cmu.edu](mailto:litster@andrew.cmu.edu) (S. Litster).

**Nomenclature**

$A$	area
$a$	pore radius
$E$	electric field
$f$	finite-thickness EDL integral parameter for flow rate
$g$	finite-thickness EDL integral parameter for flow rate per current
$I$	current
$K$	shape parameter
$L$	thickness
$\Delta p$	pressure load
$Q$	flow rate
$U$	velocity
$V$	voltage
$\varepsilon$	permittivity
$\mu$	viscosity
$\sigma$	conductivity
$\tau$	tortuosity factor
$\psi$	porosity
$\zeta$	zeta potential

**Subscripts**

EO-1	electroosmosis of the first kind
EO-2	electroosmosis of the second kind

the desired non-linear increase in flow. However, as Mischchuk et al. [8] note, the use of beads creates large macro-scale voids, or macropores ( $>10 \mu\text{m}$ ) between the beads, and limits the pressure load the pump can sustain. The flow rate of this particular pump was even reduced by the pressure load of the viscous resistance due to the micro-channel housing. Research on porous glass EO pumps has shown that pore diameters less than  $2 \mu\text{m}$  are necessary to meet the pressure loads of many practical pumping applications [1,9]. This small pore requirement for pressure capacity is a major advantage of EO pumps based on porous substrates over those with micro-fabricated channels or beads, since it is much more challenging to fabricate an equivalent number of micron-scale or sub-micron-scale channels than a porous substrate.

In this paper, we outline an engineering model of EO-2 pumping in mesoporous silica skeletons and present an experimental analysis. To the best of our knowledge, this is the first study to examine the use of electroosmosis of the second kind in mesoporous skeletons for micro-pumping applications. The modeling and experiments focus on the previously unexplored effect of intermediate pressure loads on flow rate with mesoporous skeletons. We also evaluate the scaling of EO-2 flow rate per power with miniaturization.

**2. Theory****2.1. Flow rate in mesoporous skeletons**

The overall flow within mesoporous skeletons is a combination of EO-1, EO-2, and pressure-driven flow. Here we employ a model for EO-1 flow rate that was previously applied by Yao and Santiago to porous glass EO pumps [9]. The porous EO pump was modeled as an array of tortuous capillaries, which can be individually modeled with the flow rate and current expressions developed by Rice and Whitehead [10] for a single capillary with finite EDL thickness effects. As presented in Yao and Santiago [9], the EO-1 flow rate of a porous glass pump,  $Q_{EO1}$ , is a linear function of the electric field,  $E$ , and pressure load,  $\Delta p$ . In other words, the flow rate is the linear

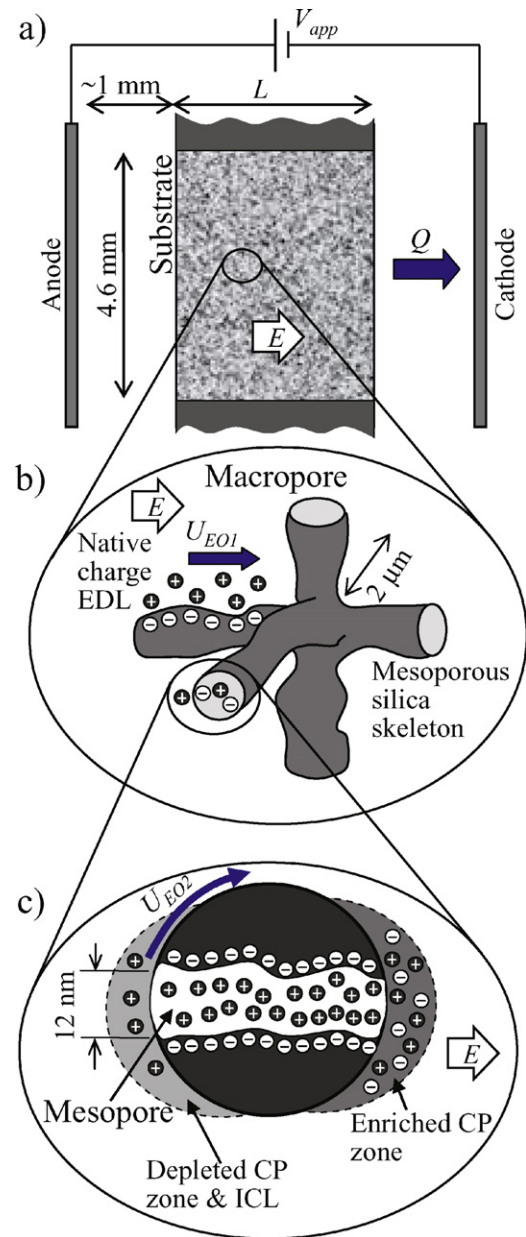


**Fig. 1.** Schematic of the EO pump structure. (a) The macroporous substrate is placed between two electrodes that apply the electric field. (b) The mesoporous skeleton forms the macropores. (c) The mesoporous structure represented as a single mesopore. Significant EDL overlap in the mesopores causes anion exclusion and the development of depleted and enriched zones at the anodic and cathodic interfaces, respectively, with an applied electric field. At high electric fields, the ICL forms on the anodic interface.

superposition of the EO flow and the reverse pressure-driven flow:

$$Q_{EO1} = A \frac{\psi}{\tau} \left[ -\frac{a^2 \Delta p}{8 \mu L} - \frac{\varepsilon \zeta E f}{\mu} \right] \quad (1)$$

where  $A$ ,  $\psi$ ,  $\tau$ ,  $a$ , and  $L$  are the area, macropore porosity, tortuosity factor, macropore radius, and thickness of the porous substrate, respectively, and  $\mu$  and  $\varepsilon$  are the viscosity and permittivity of the working fluid, respectively. The factor  $f$  is a non-dimensional parameter that accounts for finite EDL thickness in the macropores [9,10]. The zeta potential  $\zeta$  is the potential difference in the fluid between the bulk fluid and the effective hydrodynamic wall of the pore. The maximum flow rate ( $\Delta p=0$ ) of an EO pump that uses

EO-1 flow is approximated by:

$$Q_{EO1}^{\max} = -A \frac{\psi}{\tau} \frac{\varepsilon \zeta E}{\mu} f \quad (2)$$

To the best of our knowledge, there are no existing models for the EO-2 flow in a mesoporous skeleton. The lack of a model is in part due to the significant complexities associated with modeling these non-linear electrokinetic flows. Alternatively, Dukhin and Mishchuk [11–13] developed a model for the electrophoretic EO-2 velocity of an ion-permeable spherical particle. Herein, we use their model to approximate EO-2 within mesoporous skeletons. Mishchuk et al. [8] similarly used this electrophoretic velocity to approximate the EO-2 flow rate of their mesoporous bead pump [8]. As Mishchuk and Dukhin [14] present, the EO-2 velocity is an angular function over a particle's surface with a maximum velocity at the 45° point on the upstream hemisphere of the particle. The average velocity induced by EO-2 around a spherical particle can be obtained by integrating the local EO-2 velocity and is a non-linear function of electric field and particle radius [14]:

$$V_{EO2} = \frac{K \varepsilon E^2 a}{\mu} \quad (3)$$

where  $K$  is a constant related to the particle's shape. For a spherical particle, the value of  $K$  is between 5/7 [8] and 16/27 [8,15]. In Eq. (3), we observe the quadratic dependence of the velocity on the electric field. Similar to the approach of Yao and Santiago, we can roughly approximate the maximum flow rate of a porous EO pump with only EO-2 flow by the expression:

$$Q_{EO2}^{\max} = A \frac{\psi}{\tau} \frac{K \varepsilon E^2 a}{\mu} \quad (4)$$

The use of Eq. (3) to evaluate the EO-2 velocity in a pore for Eq. (4) is reasonable under the condition of thin charge layers (relative to the macropore diameter) given the identical expressions for electrophoretic particle velocity and electroosmotic velocity for EO-1 with thin EDLs. Herein, we use the idealized EO-2 model derivations for particles in Eqs. (3) and (4) to characterize the EO-2 flow rate in the mesoporous skeleton and provide engineering guidance to the design of EO-2 pumps. To apply the model, we have assumed the particle radius in Eq. (4) and pore radius are equivalent length scales. By taking the ratio of the maximum EO-2 and EO-1 flow rates, we find an expression to evaluate the significance of EO-2 flow:

$$\frac{Q_{EO2}^{\max}}{Q_{EO1}^{\max}} = \frac{KEa}{\zeta f} \quad (5)$$

Since the product  $|\zeta f|$  typically has values between 10 and 100 mV, this ratio suggests the value of the product  $Ea$  should be larger than 1–20 mV before observing significant increases in maximum flow rate from EO-2. As the electric field is inversely proportional to thickness (for constant applied voltage), significant enhancement of flow rate with EO-2 can be achieved if the substrate is made very thin. Care must be taken when inferring the role of  $\zeta$  in the denominator of Eq. (5). It appears that the enhancement is greater with lower values of  $\zeta$ ; however, the zeta potential is related to the surface charge responsible for the ion-permeability of the mesopores. CP and the ICL cannot form and no flow rate enhancement is possible without sufficient ion-permeability.

We now present an approximation for the flow rate of an EO pump with a mesoporous skeleton obtained for the transition regime where both EO-1 and EO-2 are significant by superposing the EO-1, EO-2, and pressure-driven flow rates:

$$Q_{EO2} = A \frac{\psi}{\tau} \left[ -\frac{a^2 \Delta p}{8 \mu L} - \frac{\varepsilon \zeta E}{\mu} f \left( 1 + \frac{KEa}{\zeta f} \right) \right] \quad (6)$$

The expression above assumes that the electric field driving EO-1 is tangential to the skeleton surface and is not altered by the mesopore conductivity of the mesoporous skeleton. This may be a poor assumption for low electric fields because the high charge density in the mesopores results in high conductivity; thus, electric field lines would tend to penetrate the walls of the macropores. When the electric field lines are not tangential to the pore wall, the commonly used assumption of the similarity between electric field and velocity [16] is not applicable. However, at moderate to high electric fields, the penetration of electric field lines should be significantly reduced by the low conductivity depletion region that develops on the anode side interface. The low conductivity depletion region will divert the electric field lines around the mesoporous media and increase the proportion of the electric field that's tangential to the mesoporous skeleton's surface. In addition, Eq. (6) neglects the flow generated within the mesopores because of their small hydraulic diameters.

Another significant assumption of Eq. (6) is the lack of interactions between the pressure-driven flow and both CP and EO-2 flow. Ehlert et al. [17] studied the disturbance of the CP zone surrounding a single 175  $\mu\text{m}$  mesoporous particle when an electric field was applied in a closed cell (zero net flow rate). The disturbance of the CP zones was due to the reverse pressure-driven flow mass-balancing the forward direction EO flow. However, the effect of intermediate pressure loads has not been examined in the current literature.

In the following experimental analysis, we evaluate the effect of intermediate pressure loads on EO-2 flow and the scaling of flow rate per power with substrate thickness. The pressure load effect is investigated by a parametric study of pressure loads between zero pressure load and maximum pressure (no net flow). We also evaluate the validity of the assumption in Eq. (6) that reverse pressure-driven flow does not disturb the ICL and the EO-2 flow rate.

## 2.2. Flow rate per power scaling

We now evaluate scaling EO pumps to microscale applications by examining the scaling of flow rate per power ( $Q/P$ ) with constant voltage. We compare the scaling of both EO-1 and EO-2 pumps to identify their relative merits. For both EO-1 and EO-2 pumps, the power scales as:

$$P = \frac{V_{app}^2}{R} \propto \frac{V_{app}^2 A}{L} \quad (7)$$

where  $R$  is the resistance and  $V_{app}$  is the applied voltage. From Eqs. (2) and (4), we see that the EO-1 maximum flow rate is proportional to area and electric field,  $Q \propto AE$ , whereas the EO-2 maximum flow rate is proportional to area and the electric field squared,  $Q \propto AE^2$ , where electric field is defined as  $E = V/L$ . Thus, the flow rate per power for EO-1 scales as:

$$\left. \frac{Q}{P} \right|_{EO1} \propto \frac{1}{V_{app}} \quad (8)$$

and for EO-2 it scales as:

$$\left. \frac{Q}{P} \right|_{EO2} \propto \frac{1}{L} \quad (9)$$

Eqs. (8) and (9) suggest that the flow rate per power scales inversely with voltage for EO-1 flow but scales inversely with substrate thickness for EO-2 flow. This scaling of EO-2 flow rate per power suggests significant performance enhancement with miniaturization. Note, the  $1/V$  scaling of EO-1 suggests diminishing flow rate per power when the flow rate is increased by applying greater voltage. The EO-2  $Q/P$  scaling does not exhibit this unfavorable voltage dependence.

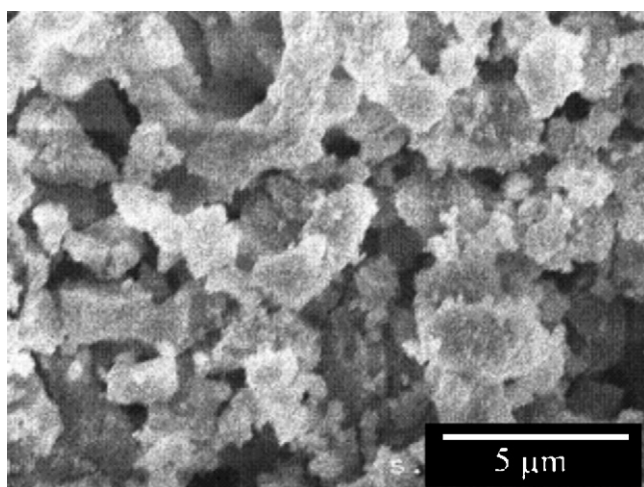


**Fig. 2.** SEM image of the porous silica substrate. The image shows the substrate surface after cutting the column section to the desired length.

For constant current conditions, the  $Q/P$  ratios for EO-1 and EO-2 flows scale as  $A/L$  and  $1/L$ , respectively. Thus, for constant current (entailing constant flow rate as well), the  $Q/P$  ratio improves for both flows when reducing thickness. However, EO-1's scaling of  $Q/P|_{EO1} \propto A/L$  shows unfavorable scaling with miniaturization of area. As area decreases, so does the flow rate per power. The EO-2 scaling shows no unfavorable scaling with area miniaturization. Thus, our scaling suggests EO-2 is potentially the superior pumping mechanism for miniaturizing EO pumps.

### 3. Materials and methods

Our EO pump design is similar to those used to study EO pumping with EO-1 [18,19]. Instead of a porous glass frit, our pump was assembled with a commercial mesoporous silica skeleton (Chromolith Performance monolithic columns, Merck KGaA, Germany) used in high performance liquid chromatography. The 4.6 mm diameter column, clad in polyether ether ketone (PEEK), was cut to desired lengths using a slitting saw. Substrates with thicknesses of 1, 1.6, 2, 2.5, 3 and 3.75 mm were prepared. Fig. 2 shows a scanning electron microscope (SEM) image of the substrate surface after cutting, depicting the macropore morphology. The mean macropore diameter of this material is  $1.9 \mu\text{m}$  and the mean mesopore diameter is  $12.5 \text{ nm}$  [20]. The macropore porosity is 60% and the mesopore porosity is 66%, corresponding to a total porosity of 86% [20].

Each substrate was placed at the center of a 1.5 mm thick acrylic sheet and sealed along the perimeter with 5 min epoxy (Devcon, Danvers, MA). The acrylic sheet was inserted in the pump housing, which was machined from Teflon. Platinum mesh electrodes (Goodfellow Cambridge Limited, UK) with 0.06 mm diameter wires and center-to-center spacings of 0.25 mm were placed on either side of the substrate with spacings of approximately 1 mm. Compressed O-ring fittings sealed the compartments on either side of the substrate.

In our experiments, we used 1 mM and 2 mM borate solution as the working electrolyte. The solution was prepared from sodium tetraborate ( $\text{B}_4\text{Na}_2\text{O}_7 - 99.5\%$ ) (Acros Organics, Morris Plains, NJ) and DI water (Fisher Scientific, Pittsburgh, PA). As measured using a combined conductivity/pH meter (Oakton pH/CON 510, Vernon Hills, IL), the average conductivity of the 1 mM solutions prepared was  $98 \pm 10 \mu\text{S/cm}$  and the pH was  $8.9 \pm 0.1$ . The 2 mM solution had a conductivity of  $180 \mu\text{S/cm}$  conductivity and a pH of 9.8. The high pH solution was used since the zeta potential of silica asym-

ptotes to a constant, high value at high pH and is constant within roughly 10% down to a pH of 7 [21]. The platinum electrodes of the pump were connected to a sourcemeter (Keithley 2410 1100 V Sourcemeter, Cleveland, OH) to apply the electric field for the pump. The borate buffer was pumped from the housing into a micro-flowmeter (Sensirion ASL1600-10 Liquid Flow Sensor, Westlake Village, CA) and then to a variable-height reservoir. For maximum pressure measurements, a pressure transducer (Omegadyne Inc., PX-209-015G5V, Sunbury, OH) was connected to the outlet of the micro-flowmeter. The pressure transducer signal was measured with a data acquisition board (National Instruments USB-6251, Austin, TX). The system was computer controlled with LabVIEW (National Instruments LabVIEW 8.6).

Prior to experiments, we flushed the substrates overnight with 1 mM borate buffer to remove possible contaminants. We performed four sets of experiments, including measurements of galvanostatic maximum flow rate (zero pressure load), potentiostatic maximum pressure (zero flow rate), galvanostatic pump performance over a range of intermediate pressure loads, and a galvanostatic parametric study of substrate thickness. For the galvanostatic maximum flow rate experiments, we used the sourcemeter in constant current mode with the pump and reservoir filled to equal heights to avoid hydrostatic pressure loads. The maximum flow rate was measured with constant current because the flow rate per current ratio,  $Q/I$ , for EO-1 flow is constant for a given pump and solution [9]. For the potentiostatic maximum pressure experiments, we blocked the flow to the reservoir with the pressure transducer to create the zero flow rate condition. The maximum pressure is measured with constant voltage because the maximum pressure for EO-1 flow is proportional to the voltage drop across the pump substrate [9]. In the galvanostatic variable-pressure load experiments, we elevated the outlet reservoir to fixed heights to generate constant levels of hydrostatic pressure load.

In all experiments, we operated the pump for at least 150 s for each realization to achieve steady-state values. The results presented are extracted from the time-average values of the last 30 s of the 150 s dwells. To ensure that bubbles generated by electrolysis did not cause inconsistent results, the cathode (outlet) compartment was emptied and refilled for each realization. The pump reservoir on the anode side of the substrate featured an open surface that allowed bubbles to escape. Each experimental point was determined using 3–5 realizations and the mean values of those realizations are plotted in the figures. In all figures, the error bars are the 95% confidence intervals for the mean values determined using Student's  $t$ -distribution for the particular number of realizations conducted at each data point. The experiments were performed at the room temperature of  $25^\circ\text{C}$ .

### 4. Results

#### 4.1. Maximum flow rate

Fig. 3 presents the galvanostatic maximum flow rate for a 1.6 mm thick substrate for currents ranging from 0.1 to 3 mA. The flow rate of  $450 \mu\text{l/min}$  at a current of 3 mA is more than two times greater than the flow rate extrapolated from the low current linear fit. Fig. 4 shows the applied voltages measured during these galvanostatic maximum flow rate experiments. The voltage versus current data shows a roughly linear relationship, as indicated by the linear fit to the data. The voltage measurement includes the Ohmic voltage drop between the electrodes and the substrate, as well as the electrochemical over-voltages. We note that the product  $Ea$  value is roughly 15 mV when the nonlinear flow rate increase arises at approximately 1 mA. This is in agreement with the range

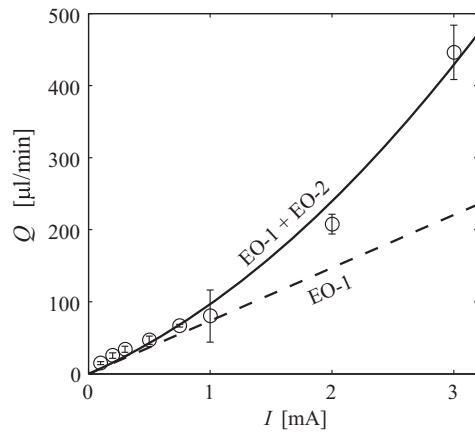
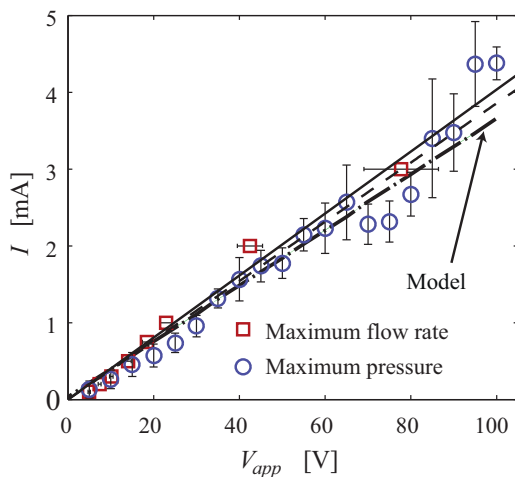


**Fig. 3.** Galvanostatic maximum flow rate for currents ranging from 0.1 to 3 mA. The error bars represent the 95% confidence intervals for the mean values of multiple realizations. The solid line (—) is the maximum flow rate predicted by the model for the combined EO-1 + EO-2 flows (Eq. (6) with  $\Delta p = 0$ ). The dashed line (---) is the EO-1 flow rate (Eq. (1) with  $\Delta p = 0$ ) determined by the model for a zeta potential found from a linear fit to the data between 0.1 and 1 mA ( $R^2$  value of 0.992).

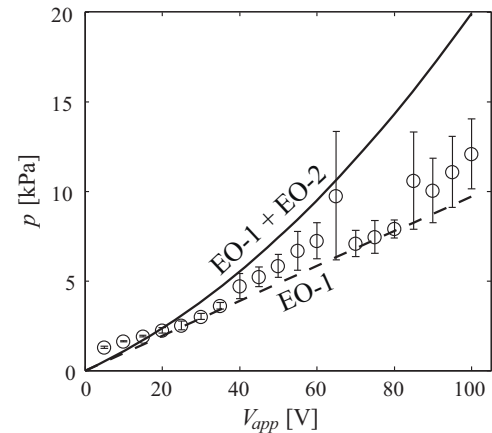
of 1–20 mV suggested by Eq. (5) for noticeable increase in flow rate due to EO-2.

Fig. 3 also presents the model predictions of the maximum flow rate for EO-1 flow (Eq. (2), dashed line) and the combination of EO-1 and EO-2 flows (Eq. (6) with  $\Delta p = 0$ , solid line). The predicted flow rate is plotted versus the current predicted with Yao and Santiago's [9] model for current at maximum flow rate,  $I = (A\psi f\sigma_{\infty}E)/(\tau g)$ , where  $\sigma_{\infty}$  is the bulk solution conductivity and  $g$  is the non-dimensional flow rate per current ratio for finite EDLs. The theoretical curve shows good agreement with the experiment and demonstrates a doubling of the flow rate at 3 mA because of the contribution of EO-2 flow. The inset of Fig. 4 shows the model prediction for the IV curve for the maximum flow rate condition, which has good quantitative and qualitative agreement with the experiment.

In applying the model, we used the actual parameter values described in Section 3 wherever possible, such as macropore and mesopore porosities, macropore diameter, thickness, and conduc-



**Fig. 4.** Voltage versus current from the galvanostatic maximum flow rate and potentiostatic maximum pressure experiments. The solid line (—) is a linear fit to the maximum flow rate data with an  $R^2$  value of 0.980 and the dashed line (---) is a linear fit to the maximum pressure data with an  $R^2$  value of 0.937. The error bars represent the 95% confidence intervals for the mean values of multiple realizations. The figure also shows the IV curve predicted by the model for the maximum flow rate condition.



**Fig. 5.** Potentiostatic maximum pressure for applied voltages ranging from 5 to 100 V. The error bars represent the 95% confidence intervals for the mean values of multiple realizations. The solid line (—) is the maximum pressure predicted by the model for the combined EO-1 + EO-2 flows. The dashed line (---) is the predicted EO-1 maximum pressure.

tivity to model the pump. The values that had to be fit from the experiment or assumed were the effective zeta potential,  $K$ , and the tortuosity factor. A zeta potential,  $\zeta$ , of  $-16.5$  mV was determined by matching the expression for EO-1 maximum flow rate per current,  $Q/I = (g\epsilon\zeta)/(\mu\sigma)$ , to the slope of a linear line fitted to the data for  $I \leq 1$  mA. The fitted  $Q/I$  slope for the low current data was  $71.9$  ( $\mu\text{l}/\text{min}$ )/mA with an  $R^2$  value of 0.992. The benefits of using flow rate per current to find the zeta potential are that all the other values in the ratio are well-established and the ratio is not dependent on material properties that are difficult to characterize, such as the tortuosity factor. Considering the 66% mesoporosity, we estimate the bulk silica/buffer solution interface zeta potential to be  $-25$  mV, assuming the effective surface charge density and zeta potential are proportional ( $\zeta = \zeta_{\text{eff}}/\psi = -16.5 \text{ mV}/0.66 = -25 \text{ mV}$ ). The macropore values of  $f$  and  $g$  were 0.959 and 0.935, respectively, which we determined using the numerical approach described by Yao and Santiago [9]. Finally, we assumed a reasonable tortuosity factor of 3 [22]. The parameter  $K$  for the EO-2 model was previously undefined for mesoporous skeletons; thus, we manually fit the value of  $K$  to match the observed quadratic increase in flow rate at higher currents. The EO-1 + EO-2 curve in Fig. 3 was obtained using a  $K$  value of 0.175. Note, a much higher theoretical  $K$  value of  $16/27$  (0.593) was previously found for EO-2 flow around a spherical ion-permselective particle [12]. Nevertheless, the present experimental  $K$  value of 0.175 and the theoretical values of  $16/27$  [8,15] and  $5/7$  [8] are of the same order of magnitude.

#### 4.2. Maximum pressure

Fig. 5 presents the potentiostatic measurements of maximum pressure versus applied voltage. At 100 V, the pump generated a maximum pressure of 12 kPa. Unlike the maximum flow rate results, the pressure data shows a more linear dependence on electric field. Fig. 4 presents the current measured during these potentiostatic experiments and compares the current–voltage curve with that from the galvanostatic maximum flow rate experiments. The current shows a linear dependence on the applied voltage. In addition, this potentiostatic current–voltage curve nearly overlaps that from the galvanostatic maximum flow rate experiments.

The dashed and solid lines in Fig. 5 show the model predictions for the maximum pressure generated by the EO-1 flow alone and the combination of EO-1 and EO-2 flow. The maximum pressure for EO-1 flow and the combined EO-1 and EO-2 flows is calculated

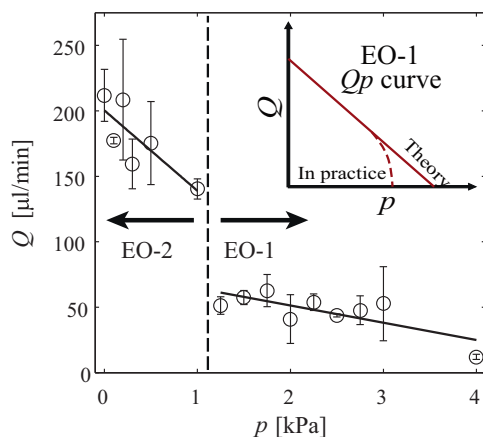


**Fig. 6.** Galvanostatic pump performance ( $Qp$ ) curve at a current of 2 mA. Two distinct regions are located at pressure loads above and below 1 kPa (approximately 20% of the maximum pressure). The solid lines are linear fits to the low pressure and high pressure regimes to guide the eye. We suggest the discontinuity is a result of the interaction between pressure-driven flow and both the ICL and EO-2 flow. The inset shows the general shape of a typical  $Qp$  curve for an EO-1 pump to illustrate the significant difference in comparison with the current EO-2  $Qp$  curve. The error bars represent the 95% confidence intervals for the mean values of multiple realizations.

by setting the flow rate to zero in Eqs. (1) and (6), respectively, and solving for  $\Delta p$ . The EO-1 flow curve shows the expected linear behavior for macroporous glass EO pumps. The theoretical curve for the combined flows shows a quadratic increase in maximum pressure due to the flow generated by EO-2. In general, the pressure data is linear and more closely follows the theoretical EO-1 curve. We note that the good agreement between the model predictions and the experimental data supports the validity of the fitting values found with maximum flow rate data.

#### 4.3. Intermediate pressure load

Fig. 6 presents a galvanostatic pump performance curve ( $Qp$  curve) at a current of 2 mA. The curve is a plot of flow rate versus fixed values of hydrostatic pressure load. The plot shows two distinct zones with a sharp discontinuity at roughly 1 kPa. The 1 kPa pressure load is approximately 20% of the maximum pressure at 2 mA. We observe that the flow rate is significantly higher at lower pressure loads. In Fig. 6, we include linear fits in the  $p \leq 1$  kPa and  $p > 1$  kPa regions of the curve. The linear fit to the data below 1 kPa is steeper and intercepts the flow rate axis at much higher values (approximately two times greater than that for the data above 1 kPa). The  $Qp$  curve measured for this pump is considerably different to that of an EO-1 pump and suggests a non-constant EO flow contribution to the total flow rate. As the inset in Fig. 6 shows, EO-1 pumps typically exhibit a linear pump performance curve from maximum flow rate to maximum pressure (constant voltage or current) without discontinuities [23]. Also, in practice, the slope of an EO-1  $Qp$  curve can often become more negative at high pressure loads due to pH changes resulting from the low flow rate to current ratios in contrast to the flattening observed in the current result.

#### 4.4. Substrate thickness

We performed an additional set of experiments to study the galvanostatic scaling of flow rate per power with substrate thickness. Fig. 7 shows the measurements of flow rate per power for substrate thicknesses of 1, 2, 2.5, 3 and 3.75 mm. The experiments were performed at a constant current of 4 mA with a 2 mM borate buffer solution. With the 1 mm thick substrate, the pump reached a maximum  $Q/P$  ratio of 1100  $\mu\text{l}/\text{min}/\text{W}$ , almost twice the flow rate per power found with the 3.75 mm thick substrate. Thus, we observe

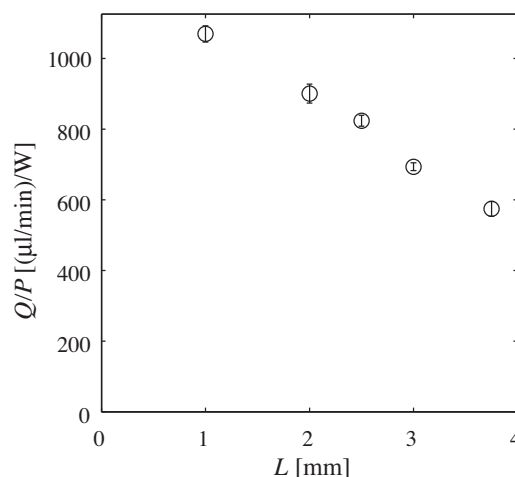


**Fig. 7.** Flow rate per power versus the substrate thickness for a constant current of 4 mA with a buffer concentration of 2 mM. The error bars represent the 95% confidence intervals for the mean values of multiple realizations.

the expected increase in  $Q/P$  with reductions in substrate thickness, but not the theoretical inverse trend.

Fig. 8 presents the model prediction of the  $Q/P$  scaling with substrate thickness for different levels of constant effective voltage (10, 30, and 100 V), which is the voltage drop across the substrate. A corresponding constant effective voltage experiment was not possible with the present apparatus because the effective voltage could not be accurately controlled due to unknown Ohmic voltage drops through the electrode spacings and the electrodes' unknown electrochemical overvoltages. Thus, we have used our model to evaluate this scaling in more detail. The model results in Fig. 8 include the predicted  $Q/P$  ratio for the EO-2 pump, as well as an EO-1 pump with the same model parameters. However, for fair comparison, the calculation for the EO-1 pump uses the estimated bulk zeta potential of  $-25$  mV and does not include a zeta potential reduction due to the EO-2 pump's mesoporosity. As expected from the scaling arguments in Section 2.2, the EO-2 pump exhibits the  $1/L$  scaling whereas the EO-1 pump has a constant value of  $Q/P$  at each voltage and decreases with greater voltages. At each voltage, the figure shows there is a cross-over thickness (circled) where further reductions in thickness result in higher flow rate per power

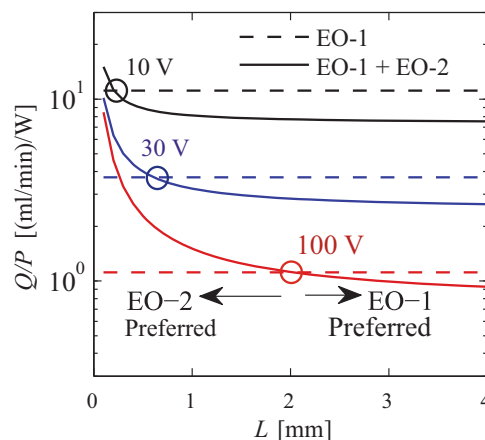


**Fig. 8.** Model predictions of flow rate per power versus substrate thickness for effective voltages (voltage drop across the substrate) of 10, 30, and 100 V. At each voltage, the  $Q/P$  ratio is given for an EO-1 pump with a bulk zeta potential of  $-25$  mV and an EO-2 pump with a lower zeta potential of  $-16.5$  mV due to the mesoporous skeleton's 66% mesoporosity. The circles indicate each voltage level and the cross-over thickness at which further reductions in thickness favor the use of an EO-2 pump.

with the EO-2 pump. The cross-over thickness increases as higher voltages are applied because of greater electric field and greater EO-2 flow at any given thickness. For the highest voltage (100 V) and the thinnest substrate (100  $\mu\text{m}$ ) considered, the model predicts an order of magnitude greater flow rate per power with the EO-2 pump versus the EO-1 pump.

## 5. Discussion

Our maximum flow rate results (see Fig. 3) exhibited the expected quadratic dependence of flow rate on electric field, which is quantitatively and qualitatively similar to that measured by Nischang and Tallarek [5] for the same material. Furthermore, we observed good agreement with the model, supporting our hypothesis of superposed EO-1 and EO-2 flow in the mesoporous skeleton. In contrast to our maximum flow rate results, the substantially more linear trends found for maximum pressure (see Fig. 5) and the discontinuity in the  $Qp$  curve (see Fig. 6) indicate that reverse pressure driven flow can significantly diminish EO-2 flow. The roughly linear maximum pressure data suggests that the ICL did not form in most of the maximum pressure experiments and that the pressure was mostly generated by EO-1. This is also indicated by the lower bound of the results closely following the EO-1 model curve for maximum pressure. This finding also provides an additional confirmation of the model parameters obtained from the maximum flow rate experiments. However, we observed large variability in the maximum pressure results, suggesting that the EO-2 flow may have been partially present in some instances.

The discrepancy in the theoretical and estimated  $K$  values, 16/27 [15] and 5/7 [8] versus 0.175, respectively, is likely due to the significant differences in geometry between the idealized spherical model and complex mesoporous skeleton geometry as well as the assumptions of linearly superposable EO-1 and EO-2 flows and the equivalence of the particle and pore length scales. The skeleton geometry is likely to reduce the overall EO-2 flow contribution over that of a particle (lowering  $K$ ) because EO-2 flow is generated on interfaces facing the cathode and the relative proportion of surface facing the cathode is less with the skeletons. For example, unlike a sphere, mesoporous skeletons have a significant number of branches parallel to the electric field, which will not generate EO-2 flow. We also note that these parameters were estimated assuming properties at 25 °C. Internal increases in temperature due to Joule heating could alter properties such as viscosity. For future research, it is recommended that temperature sensors be integrated into the pump so that the internal temperature can be used in parameter estimations.

The galvanostatic flow rate versus intermediate pressure load data in Fig. 6 showed two distinct regimes of pump operation, determined by the magnitude of the pressure load. The two regimes are separated by a sharp discontinuity, suggesting that there is a critical pressure load at which the effect of EO-2 is diminished by the reverse pressure-driven flow. We hypothesize that the reverse flow is thinning the depletion concentration boundary layer by the advection high concentration solution from the cathode side, which would increase the ion concentration in the depletion region and lessen the induced charge. This observation deserves further fundamental analysis in future work. In addition, this phenomenon should be carefully considered when pumping with EO-2 flow in mesoporous skeleton substrates. For example, an EO-2 micro-pump would need to be specified with special consideration to ensure the peak pressure load in a given application does not exceed the critical pressure load. Further research is needed to identify the dependencies of this critical pressure load.

The linear  $IV$  results in Fig. 4 suggest that the charge transport pathways through substrate did not significantly change during the

maximum flow rate or maximum pressure experiments at either high or low currents. This finding indicates that a large majority of the current is traveling through the macropores in our experiments and supports our modeling assumptions of current traveling mainly through the macropores and the electrical field being tangential at the macropore walls. This also eliminates the possibility that the non-linear maximum flow rate behavior is due to the formation of the depletion region and resulting increase of tangential electric field strength that drives EO-1 flow.

We note that in comparison to prior work on porous EO-1 pumps, the flow rate per current and maximum pressure measured with the mesoporous silica skeleton are lower over the range of currents and voltages explored. The maximum value of flow rate per current evaluated from Fig. 3 (150  $\mu\text{l}/\text{min}/\text{mA}$  at 3 mA) is roughly 20–30% of that measured for EO pumps based on macroporous borosilicate substrates with 1 mM borate buffer (500–800  $\mu\text{l}/\text{min}/\text{mA}$ ) [18,19]. As previously noted, the theoretical maximum flow rate per current for an EO-1 pump is a constant for a particular pump and solution combination and is only a function of zeta potential and conductivity for dilute aqueous solutions,  $Q/I_{EO1} \propto \zeta/\sigma$ , [18]. Our lower EO-2  $Q/I$  values are likely due to the mesoporous silica substrate's low surface charge density and resulting low zeta potential, as indicated by the fitted zeta potential of  $-16.5$  mV that suggests a bulk zeta potential of  $-25$  mV, when considering the 66% mesoporosity. In contrast, the zeta potential of borosilicate with a 1 mM borate buffer is in the range of  $-70$  to  $-90$  mV [18]. Further work is needed to resolve this difference. The low zeta potential may also be the reason for the lower maximum pressure measurements in comparison to EO-1 pumps (approximately half of typical  $\Delta p_{\text{max},EO1}$  values) [18,19].

Fig. 7 illustrates the expected increase of flow rate per power with decreasing substrate thickness, further demonstrating an opportunity for EO micropumps with significantly greater flow rate per power with miniaturization. Our thinnest substrate (1 mm thick) achieved a flow rate of 1100  $\mu\text{l}/\text{min}$  at 4 mA constant current. Significantly thinner substrates are feasible; for example, Vajandar et al. [24] successfully demonstrated EO-1 pumps with substrates as thin as 90  $\mu\text{m}$ . For the substrate thicknesses of 2.5, 3, and 3.75 mm, we observed a slight inverse trend in Fig. 7. However, we did not observe the expected inverse trend for  $Q/P$  scaling with the thinner substrates (1–2.5 mm) and instead observed diminished increases in flow rate per power with decreasing thickness. We believe this difference is due to the constant electrode spacing in our pump housing. As thinner substrates are used, the approximately constant electrode spacing causes a greater portion of the applied potential to be dropped over the electrode/substrate spacings, rather than over the substrate. In addition, the condition of the outer substrate surfaces may play a more dominant role with thinner substrates. In future work, we plan to investigate using integrated electrodes to eliminate the electrode spacing and enable thinner EO-2 pumps with higher flow rate per power.

Another important figure of merit for evaluating pump performance is efficiency, which is a function of flow rate, pressure load, and power;  $\eta = Qp/V_{\text{app}}I$ . Thus, the efficiency value depends on the operating point within the pump performance curve. To avoid ambiguity, Laser and Santiago [1] used an efficiency metric based on linear pump performance curves to compare micro-pumps, which estimates the maximum efficiency when the pressure load and the flow rate are half of their maximum values. This efficiency metric is defined by the equation  $\eta = 0.25Q_{\text{max}}p_{\text{max}}/V_{\text{app}}I$ . We have evaluated this efficiency from our EO-2 pump's maximum flow rate and pressure data at an applied current of 3 mA ( $V_{\text{app}} \approx 80$  V) and found it to be  $6 \times 10^{-3}\%$ . This value is lower than typically reported for EO-1 pumps, such as the 0.3% value obtained by Yao et al. [19]. However, the efficiency of the EO-2 pump studied herein improves with greater applied electric fields due to the non-linear EO-2. A

22% increase in efficiency was obtained at the 3 mA operating point over that at the 2 mA ( $V_{app} \approx 43$  V) operating point. Thus, efficiency increases with greater applied voltage and thinner substrates. Also, we note that the maximum pressures used in these efficiency estimations provide conservative values for comparisons because of the diminished EO-2 flow contribution at the maximum pressure load condition.

Based on the results presented here, it is apparent that EO micro-pumps that use EO-2 in mesoporous skeletons are best suited to applications for which high flow rates are needed and high voltages are permissible. As Fig. 8 illustrates, there is a potential for an order of magnitude greater flow rate per power when using thin substrates at high voltages. Furthermore, our scaling analysis in Section 2.2 suggests the improvement with EO-2 pumps is further increased when considering pumps of smaller area. However, as Mishchuk et al. [8] discussed, operating an EO pump with DC current presents several challenges for long term operation, including bubble generation and pH change due to electrolysis reactions. These effects are particularly problematic for the high currents generated when applying high voltages across thin substrates. To mitigate these effects, Mishchuk et al. [8] demonstrated that the non-linearity of the EO-2 pump's flow rate per current enables bulk flow from an alternating current (AC) source with zero net current. With sufficiently fast AC frequencies (on the order of the electrode capacitive charging time), the generation of bubbles and pH gradients can be prevented because there is zero net Faradaic current. Thus, when properly applying a high positive voltage (high current) for a short duration and low negative voltage (low current) for a longer duration, the pump generates net flow with zero net current. This positive net flow is not possible with an EO-1 pump because the current and flow rate are linearly proportional. This same AC approach could be applied in the future to EO-2 pumps with mesoporous skeletons to provide stable long term performance. Another important avenue of future research is to evaluate the effects of the working solution's pH and ionic strength since the zeta potential and ion-permeability are sensitive to these solution properties.

## 6. Conclusion

In this paper we presented an experimental study of an EO pump using a mesoporous silica skeleton to pump liquids with EO-2. The focus of the study was the influence of reverse pressure-driven flows (due to pressure loads) on the performance of these pumps, and the effect of substrate thickness on flow rate per power. Our study included measurements of galvanostatic maximum flow rate, potentiostatic maximum pressure, galvanostatic flow rate versus fixed hydrostatic pressure load (pump performance curve), and flow rate per power for various thicknesses. The maximum flow rate experiments exhibited the expected quadratic dependence of flow rate on electric field. The measurements of galvanostatic flow rate versus applied hydrostatic pressure load showed a significant and sharp decrease in flow rate as the pressure load increased above 20% of the maximum pressure. This result and the measured linear dependence of maximum pressure on voltage indicate that significant reverse pressure-driven flow can extinguish the ICL and prevent EO-2. This must be accounted for when designing an EO pump that leverages EO-2. Galvanostatic flow rate per power measurements and modeling showed significant improvement with thinner substrates and the potential benefits of miniaturizing of EO-2 pumps that use mesoporous skeletons.

## Acknowledgements

The authors gratefully acknowledge U. Tallarek for providing the mesoporous silica material.

## References

- [1] D.J. Laser, J.G. Santiago, A review of micropumps, *J. Micromech. Microeng.* 14 (2004) R35–R64.
- [2] K.E. Goodson, J.G. Santiago, T. Kenny, L. Jiang, S. Zeng, J.-M. Koo, L. Zhang, S. Yao, E. Wang, Electroosmotic microchannel cooling system for microprocessors, *Electron. Cooling* 8 (2002) 46–47.
- [3] S. Litster, C.R. Buie, T. Fabian, J.K. Eaton, J.G. Santiago, Active water management for PEM fuel cells, *J. Electrochem. Soc.* 154 (2007) B1049–B1058.
- [4] S. Litster, B. Ha, D. Kim, J.G. Santiago, Two-liquid electroosmotic pump for portable drug delivery systems, in: *International Mechanical Engineering Congress and Exposition*, Seattle, WA, 2007, pp. 963–964.
- [5] I. Nischang, U. Tallarek, Nonlinear electroosmosis in hierarchical monolithic structures, *Electrophoresis* 25 (2004) 2935–2945.
- [6] S.S. Dukhin, N.A. Mishchuk, Intensification of electro dialysis based on electroosmosis of the 2nd kind, *J. Membr. Sci.* 79 (1993) 199–210.
- [7] I. Nischang, A. Hölzel, A. Seidel-Morgenstern, U. Tallarek, Concentration polarization and nonequilibrium electroosmotic slip in hierarchical monolithic structures, *Electrophoresis* 29 (2008) 1140–1151.
- [8] N.A. Mishchuk, T. Heldal, T. Volden, J. Auerswald, H. Knapp, Micropump based on electroosmosis of the second kind, *Electrophoresis* 30 (2009) 3499–3506.
- [9] S.H. Yao, J.G. Santiago, Porous glass electroosmotic pumps: theory, *J. Colloid Interface Sci.* 268 (2003) 133–142.
- [10] C.L. Rice, R. Whitehead, Electrokinetic flow in a narrow cylindrical capillary, *J. Phys. Chem.* 69 (1965) 4017–4024.
- [11] S.S. Dukhin, N.A. Mishchuk, Concentration polarization of conducting particle in strong fields, *Colloid J. USSR* 52 (1990) 390–393.
- [12] S.S. Dukhin, N.A. Mishchuk, A.A. Tarovskii, A.A. Baran, Electrophoresis of the 2nd Kind, *Colloid J. USSR* 49 (1987) 544–545.
- [13] N.A. Mishchuk, S.S. Dukhin, Space-charge of a conducting particle in the over-limit current regime, *Colloid J. USSR* 52 (1990) 427–431.
- [14] N.A. Mishchuk, S.S. Dukhin, Electrokinetic phenomena of the second kind, in: A.V. Delgado (Ed.), *Interfacial Electrokinetics and Electrophoresis*, Marcel Dekker, Inc., 2002, pp. 241–275.
- [15] N.A. Mishchuk, S. Barany, A.A. Tarovsky, F. Madai, Superfast electrophoresis of electron-type conducting particles, *Colloids Surf. A* 140 (1998) 43–51.
- [16] J.G. Santiago, Electroosmotic flows in microchannels with finite inertial and pressure forces, *Anal. Chem.* 73 (2001) 2353–2365.
- [17] S. Ehlert, D. Hlushkou, U. Tallarek, Electrohydrodynamics around single ion-permeable glass beads fixed in a microfluidic device, *Microfluid. Nanofluid.* 4 (2008) 471–487.
- [18] D. Kim, J.D. Posner, J.G. Santiago, High flow rate per power electroosmotic pumping using low ion density solvents, *Sens. Actuators A* 141 (2008) 201–212.
- [19] S.H. Yao, D.E. Hertzog, S.L. Zeng, J.C. Mikkelsen, J.G. Santiago, Porous glass electroosmotic pumps: design and experiments, *J. Colloid Interface Sci.* 268 (2003) 143–153.
- [20] F.C. Leinweber, D. Lubda, K. Cabrera, U. Tallarek, Characterization of silica-based monoliths with bimodal pore size distribution, *Anal. Chem.* 74 (2002) 2470–2477.
- [21] B.J. Kirby, E.F. Hasselbrink, Zeta potential of microfluidic substrates: 1. Theory, experimental techniques, and effects on separations, *Electrophoresis* 25 (2004) 187–202.
- [22] E.L. Cussler, *Diffusion – Mass Transfer in Fluid Systems*, Cambridge University Press, New York, 1997.
- [23] S.H. Yao, A.M. Myers, J.D. Posner, K.A. Rose, J.G. Santiago, Electroosmotic pumps fabricated from porous silicon membranes, *J. Microelectromech. Syst.* 15 (2006) 717–728.
- [24] S.K. Vajandar, D.Y. Xu, D.A. Markov, J.P. Wikswo, W. Hofmeister, D.Y. Li, SiO<sub>2</sub>-coated porous anodic alumina membranes for high flow rate electroosmotic pumping, *Nanotechnology* 18 (2007) 1–8.

## Biographies

**Fevzi C. Kivanc** received his B.S. degree in Mechanical Engineering from Istanbul Technical University in 2008 and received his M.S. degree in Mechanical Engineering from Carnegie Mellon University in 2010. His research interests are mainly in thermo-fluids, including electrokinetics, electrochemistry, HVAC systems, fire dynamics and protection and renewable energy.

**Shawn Litster** is an Assistant Professor in the Department of Mechanical Engineering at Carnegie Mellon University. He received his Ph.D. in Mechanical Engineering from Stanford University and received his B.Eng. and M.A.Sc. degrees from the University of Victoria. His research focus is micro- and nano-scale transport phenomena in energy conversion technologies where electrochemistry and electrokinetic effects are dominant, such as fuel cells. The research includes sensors for micron-scale measurements in porous electrodes and fabrication and analysis of hierarchical porous media. He has over 28 peer-reviewed publications, including 14 journal articles and two book chapters, as well as three pending patents.